Journal of
Ceramic Science
and Technology

J. Ceram. Sci. Tech., **05** [03] 203-208 (2014)
DOI: 10.4416/JCST2014-00008
available online at: http://www.ceramic-science.com

Yttrium Disilicate Micro-Cellular Architecture from Biotemplating of Luffa Cylindrica

S.C. Santos*[1], C. Yamagata[1], A.C. Silva[1], L.F.G. Setz[2], S.R.H. Mello-Castanho[1]

[1]Nuclear and Energy Research Institute, IPEN-CCTM, 2242 Lineu Prestes Avenue. University City, 05508000, São Paulo, SP, Brazil
[2]Federal University of ABC, Center for Engineering, Modeling and Applied Social Science,5001 Do Estado Avenue. Santo André, 09210 – 580, SP, Brazil

received February 24, 2014; received in revised form May 15, 2014; accepted June 13, 2014

Abstract

The aim of this study consists in producing porous yttrium disilicate components by using Luffa Cylindrica vegetable sponge as a template for the replica method. With consideration of the effectiveness of additives, solids content and pH, the rheological behavior of yttrium disilicate aqueous suspensions was evaluated. Stabilization of the suspensions was achieved with an electrostatic mechanism using tetraethylammonium hydroxide and with an electrosteric mechanism by adding polyacrylic ammonium salt. Shear thinning suspensions were prepared by adding 2 wt% polyelectrolyte, pH 10, and 0.4 wt% binder. This condition promoted reliable impregnation results as well as improved mechanical strength of impregnated sponges. The sintering of impregnated samples at 1500°C/7 h resulted in porous components with a morphology similar to biotemplated micro-cellular architecture and a density of 3.21 g·cm^{-3} that corresponds to 80 % of theoretical density (4.04 g%·cm^{-3}). Thermoluminescence characterization of yttrium disilicate powders showed that whole light emission occurred in the infrared range (λ = 750 – 4300 nm), with the wavelength at 1000 nm at 400 °C.

Keywords: Disilicate, ceramic processing, luminescence, porous ceramic, rheology.

I. Introduction

Rare earth disilicates (RE_2SiO_2) have been studied because of their magnetic, electric and optical properties. Yttrium disilicate ($Y_2Si_2O_7$) exhibits important structural properties such as refractoriness (melting point of 1775 °C) and stability in an oxidant environment. This compound has five polymorphs, being classified by Ito *et al.*[1] as $\alpha \xrightarrow{1225^\circ C} \beta \xrightarrow{1445^\circ C} \gamma \xrightarrow{1535^\circ C} \delta$. In addition, Bataliev *et al.*[2]reported that the fifth polymorph y (Yttrialite) is stable up to 1200 °C.

Previous works[2–12] on material synthesis were mainly focused on the preparation of $Y_2Si_2O_7$ powders by means of the sol-gel[13], hydrothermal[14] and solid-state reaction methods[15]. Owing to the difficulties associated with the preparation of this compound, colloidal processing of $Y_2Si_2O_7$ has not yet been investigated. Controlling the stability of dispersed particles in an aqueous medium is an important parameter to prepare suitable suspensions for the shape-forming process. Consequently, near-net-shape components exhibiting reliable characteristics can be produced[16–19].

The concept of a gas burner for lighting was presented by Takeno and Sato[20, 21]. With the use of a porous component, it was possible to sustain a flame with lower fuel rates. The combustion of a mixture of air and fuel (natural gas, ethanol, and biogas) in the porous burner can be divided into three steps. Reflux zone (1), the gas is hotter than the ceramic structure and as a result, the heat is conducted by convection from the combustion zone to the porous ceramic structure; ceramic conduction (2), the ceramic structure conducts and irradiates the heating flow to the combustion zone; heating of the gas (3), in this step the temperature of the ceramic structure is higher than the gas and the heat is conducted by a convection process based on a solid-vapor system. In this way, the entrance gases are preheated up to the limit temperature in order to start the reaction and maintain the cycle. This condition improves the stability of the flame and also the efficiency of the combustion, resulting in lower emission of greenhouse gases[22].

Replica is a shape-forming process to produce complex-shaped components from ceramic suspensions and an organic template[23–29]. For this process two aspects are very important, (1) the ceramic suspension has to exhibit shear thinning behavior[30] in order to cover the template surface uniformly, (2) thermal treatment of impregnated template has to be performed at a slow heating rate so that the organic template can be burned out without disrupting the ceramic structure. Literature shows that the most commonly used templates are wood[31], carbon sponge[32], polyurethane foam[33], vegetable sponge[34] and other natural fibers[35–37].

Among the vegetable structures, the sponge gourd is a fruit of the Luffa (Aegyptica or Cylindrica) with a natural cellular architecture that is interesting for gas burner de-

* Corresponding author: silas.cardoso@usp.br

sign. The vegetable fibers are arranged in a multidirectional way, forming a mat. This architecture can improve gas burning and light emission efficiency based on both heat circulation and gas restriction inside its structure.

By means of hydrothermal synthesis at environmental pressure, Diaz *et al.*[14] successfully prepared β-$Y_2Si_2O_7$:Dy^{3+}, the light emission of which closely corresponded to 40 % of Y_2O_3:Eu^{3+}. Therefore, with regard to the potential of $Y_2Si_2O_7$ for luminescent applications, this work aims to evaluate the colloidal processing of β-$Y_2Si_2O_7$.

In this paper, we evaluate the rheological behavior of β-$Y_2Si_2O_7$ aqueous suspensions by controlling the surface condition of particles. Shear thinning suspensions suitable for replicating the vegetable sponge structure were prepared. Porous yttrium disilicate components with potential for use as gas burners for lighting were produced.

II. Experimental

Beta yttrium disilicate (DsY) was produced with the hydrothermal method based on Diaz *et al.*[14], real density (ϱ) of 4.04 $g{\cdot}cm^{-3}$ and specific surface area (SSA) of 10.9 $m^2{\cdot}g^{-1}$.

The mean particle diameter was measured by means of photon correlation spectroscopy (PCS, ZetaPALS Analyzer, Brookhaven Instruments). For PCS, an aqueous suspension with 0.01 vol% solids was prepared at pH 10 with the addition of tetraethylammonium hydroxide (TMAH, Sigma-Aldrich) as a deflocculant and homogenization of the mixture in a ball mill for 24 h.

The emitted luminescence of DsY particles was measured with a combined thermoluminescence reader (model Risø TL/OSL-DA-20) based on a heating condition up to 700 °C and a spectrometer (Ocean Optics, model QE65 Pro) with spectral sensibility from 200 to 950 nm. The samples were heated at a heating rate of 2 K/s up to 400 °C in environmental atmosphere. Afterwards, the samples were cooled in a nitrogen flow until environmental temperature was reached.

Zeta potential (ζ) in aqueous medium was evaluated with a light scattering analyzer (ZetaPALS, Brookhaven Instruments Corporation). Stock suspensions with 0.5 $g{\cdot}L^{-1}$ solids were prepared with NaCl 10^{-3}M as an indifferent electrolyte. HCl and KOH solutions were used to set the pH of the stock suspensions from acid to alkaline (pH 5.6 – 12). In addition, 0.5 to 2 wt% polyacrylic ammonium acid (PAA, Duramax D3005) was added to the stock solution. Before the measurements were conducted, all the suspensions were homogenized in an ultrasound cleaner for 2 min (Dr. Hielscher 400US).

Concentrated DsYsuspensions from 5 to 25 vol% were prepared with tetramethylammonium hydroxide (TMAH, Sigma-Aldrich), PAA from 0 – 3 wt%, carboxymethyl-cellulose (CMC, Sigma-Aldrich) from 0.3 to 1 wt% (based on the suspension weight). All suspensions were homogenized in a ball mill for 24 h, using alumina spheres ($Ø_{spheres}$=10 mm).

The flow behavior of the suspensions was evaluated with a rheometer (Haake RS600, Thermo Scientific). The sensor system consisted of a double-cone rotor and stationary plate (DC60/1°). The flow behavior of the DsY suspensions was characterized in the control rate mode (CR). Measurements were evaluated at 25 °C by increasing the shear rate from 0 to 1000 s^{-1} in 5 min, holding for 2 min at 1000 s^{-1} and returning to 0 s^{-1} in 5 min. For each CR step, 200 points were measured.

The sponge gourd (Luffa Cylindrica, LCy) was used as a template. LCy rectangular samples (30 x 30 x 5 mm) were immersed in DsY suspension for 30 min (optimized time)[38]. After the excess ceramic material had been squeezed out, the samples were dried at environmental temperature for 24 h. The impregnated samples were sintered in a vertical furnace (Lindberg/Blue M), where the thermal treatment conditions were based on thermal and gravimetric analysis (TGA/TDA) results of LCy fibers. The microstructure of the sintered samples was evaluated with scanning electron microscopy (MEV, TM 3000 Hitachi and MEV, INCAx-act Oxford Instruments).

III. Results and Discussion

The mean particle size distribution of the DsYpowders measured with PCS is shown in Fig. 1a. The yttrium disilicate powders exhibited a narrow particle size distribution with a mean diameter (d_{50}) of 97 nm. Homogeneous distribution is desirable to prepare the porous microstructure from the suspensions, since particles with similar size make voids during sedimentation. In addition, the index indicating how agglomerated the particles are, the agglomeration factor (Fag), was only 0.71. Besides, the difference between the distributions d_{10} and d_{90} was 1.3 nm (Span). Furthermore, relating Span to (d_{50}) resulted in a small difference of 0.01 (relative span), which confirms the narrow distribution of particles. As shown in the SEM (Fig. 1b) DsY powders are composed of aggregates of granular particles with mean size of 15 nm.

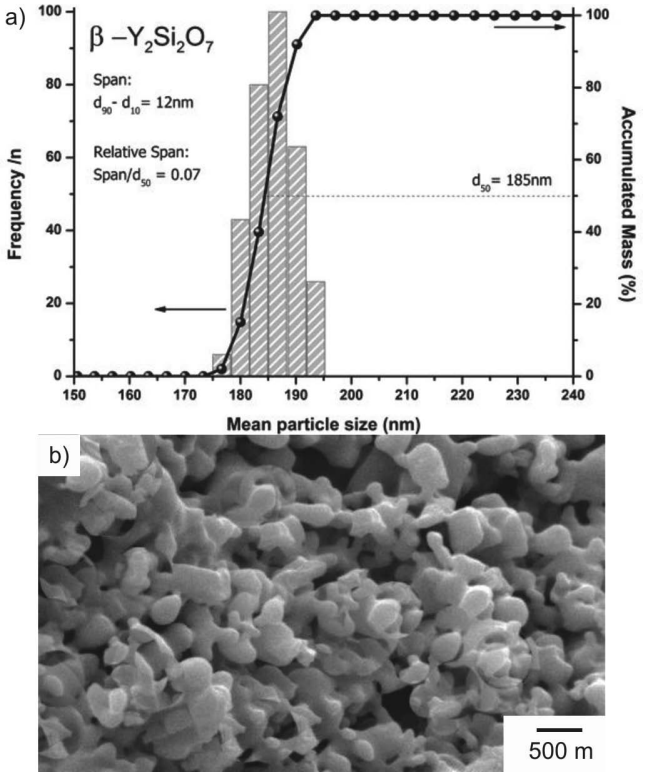

Fig. 1: Characterization of DsY powders – (a) distribution of mean particle size by PCS and (b) particle size and morphology by SEM.

Zeta potential curves of DsYas a function of pH and PAA are shown in Fig. 2. Suspensions with no dispersant exhibited the isoelectric point (IEP) at pH 7.8. The stability condition was achieved at pH 5 ($\zeta = |32mV|$), pH 6 ($\zeta = |37mV|$) and at pH ≥ 8.5, whereby the highest stability was established at pH 11 ($\zeta = |58mV|$). Concentrations of 0.5 wt% PAA were not efficient to shift the IEP and promote a larger range of pH stability. However, concentrations of PAA ≥ 1 wt% promoted a shift of the IEP from pH 7.8 to pH 6.3. As result, stability conditions ($|\zeta \geq 20mV|$) were achieved at pH ≥ 7.0, and were maximum for 2 wt% PAA at pH 10 ($|\zeta = 70mV|$). These parameters supplied the greatest stability of the particles, and in this condition concentrated suspensions can be prepared. However, using 3 wt% PAA promoted an increase in ionic strength and consequently decreased the repulsive interparticle forces.

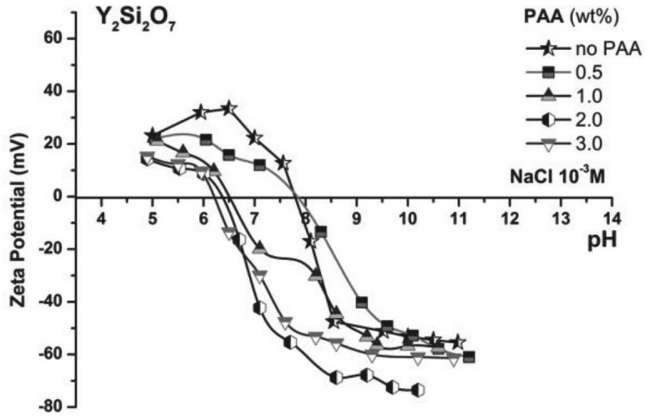

Fig. 2: Zeta potential curves of $Y_2Si_2O_7$ particles as a function of pH and PAA.

The PAA concentration has an influence on the flow behavior of DsY suspensions as shown in Fig. 3 and Fig. 4. Suspensions prepared with up to 1 wt% PAA exhibited a dilatant tendency, with viscosity increasing as a function of increasing shear stress and in this condition the flow behavior fitted with the Oswald de Waele model. With 2 wt% PAA, the dispersion was significant, the flow behavior becoming linear for both up and down curves (Fig. 3). Even though 3 wt% PAA promoted linear flow, the effectiveness stability was the same as for 2 wt% PAA (Fig. 3 and Fig. 4). Furthermore, the results can be seen as indicative of the dispersant dosage limit.

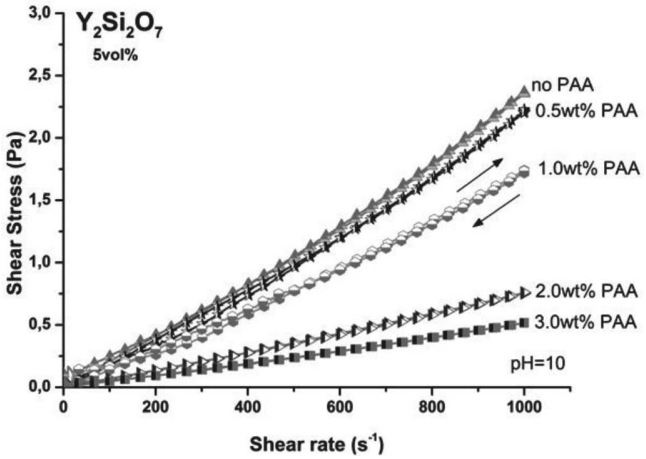

Fig. 3: Flow curves of $Y_2Si_2O_7$ suspensions with solids load from 5 – 25 vol% and prepared with 2 wt% PAA and pH 10.

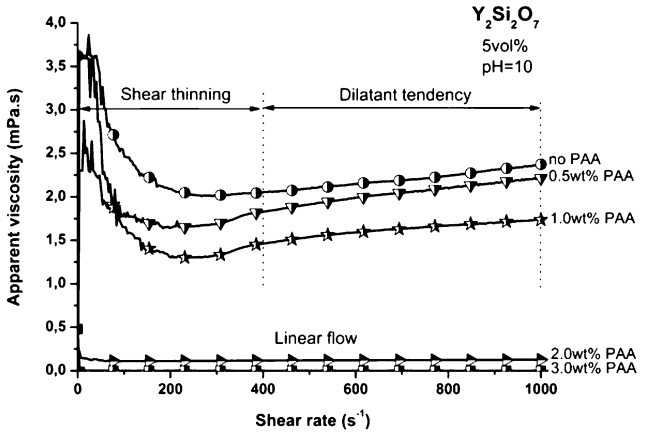

Fig. 4: Dynamic viscosity of 5 vol% $Y_2Si_2O_7$ suspensions from 0 until 1000s^{-1}. Based on PAA concentration, the suspensions showed two stages of rheological behavior: shear thinning and dilatant tendency.

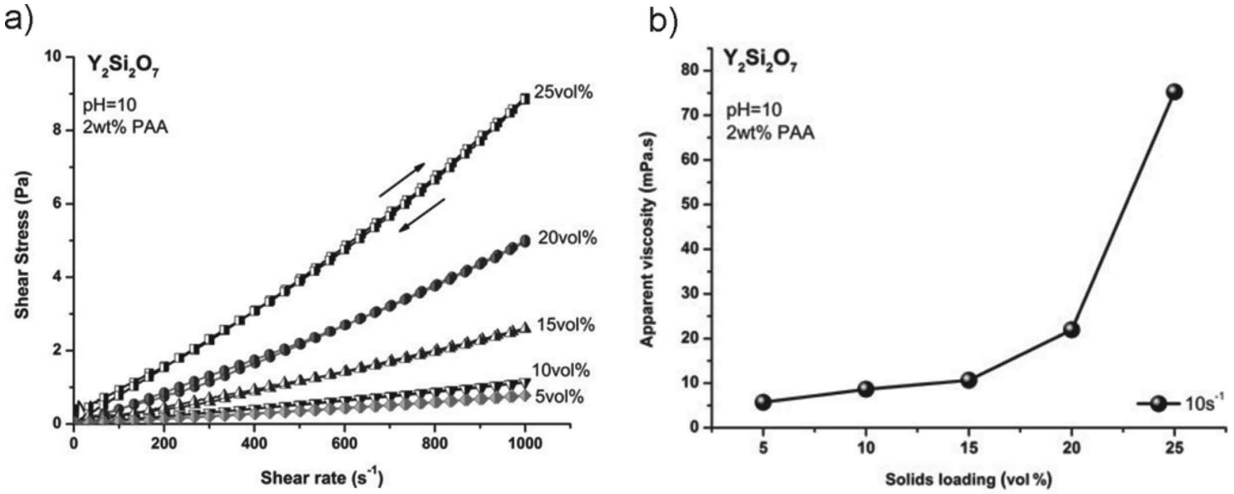

Fig. 5: Flow behavior of $Y_2Si_2O_7$ suspensions prepared with solids loading from 5 – 25 vol% up to 1000s^{-1}. (a) flow curves of $Y_2Si_2O_7$ suspensions in CR mode, (b) determination of apparent viscosity at 10s^{-1}.

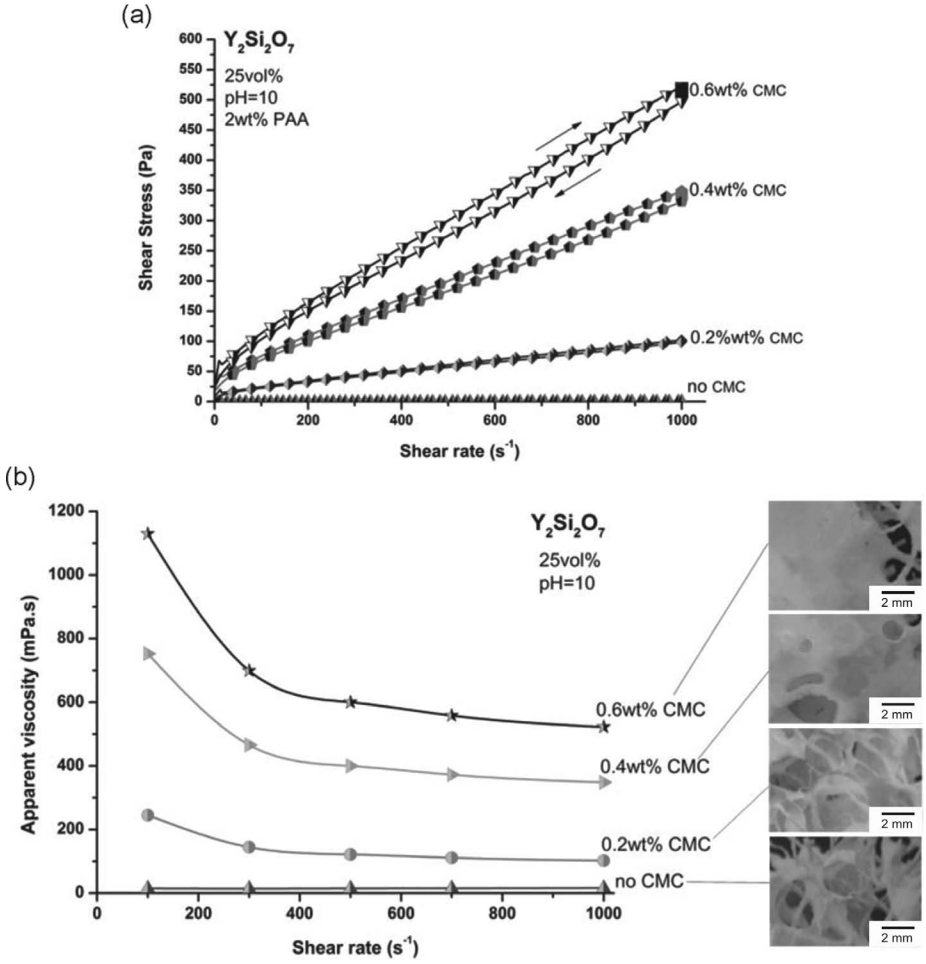

Fig. 6: Rheological behavior of 25 vol% $Y_2Si_2O_7$ as a function of CMC concentration from 0 to 0.6 wt%.(a) flow curves in CR mode, (b) variation of apparent viscosity according to shear rate from 0 to 1000s^{-1}.

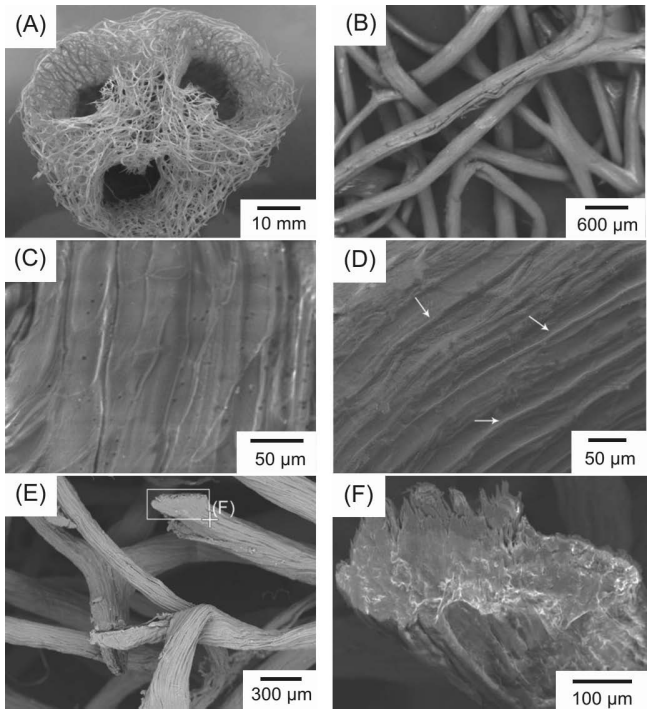

Fig. 7: Luffa Cylindrica sponge (LCy). (A) top view; (B) SEM micrograph of LCy mat fibers as received; SEM micrographs of LCy fibers' surface, (C) as received, (D) after alkaline treatment; (E) LCy fibers showing microcellular structure and (F) cross-section of the fibers of the LCy, showing the helical texture of the hollow microchannels.

Fig. 8 shows the thermal gravimetric analysis (TGA) result of a LCy template evaluated up to 800 °C in environmental atmosphere. Decomposition peaks were caused by the loss of water at 100 °C, hemicellulose degradation from 100 °C – 280 °C, cellulose degradation from 260 °C – 350 °C, and lignin degradation from 350 °C – 500 °C. A critical zone which corresponds to a substantial loss in weight (76 wt%) took place between 250 °C and 450 °C as shown by the DTG curve (dark gray line). From 500 °C, the LCy structure was totally burned out (100 wt%). Furthermore, controlled thermal treatment is fundamental in order to burn out the template structure without disrupting the ceramic phase. Based on the TGA results, the following thermal treatment conditions for impregnated templates was 1 °K/min until 1500 °C/7 h.

Untreated LCy fibers (Fig. 9a) exhibited poor yttrium disilicate adhesion. The waxy and gummy substances inhibit impregnation of the ceramic suspension into the biotemplating surface. Therefore NaOH solution is used as a wetting agent to activate the fiber surface. Consequently, a thick ceramic layer could be impregnated as shown in Figs. 9b and 9c. The mass gain was around eight times higher compared with natural fiber.

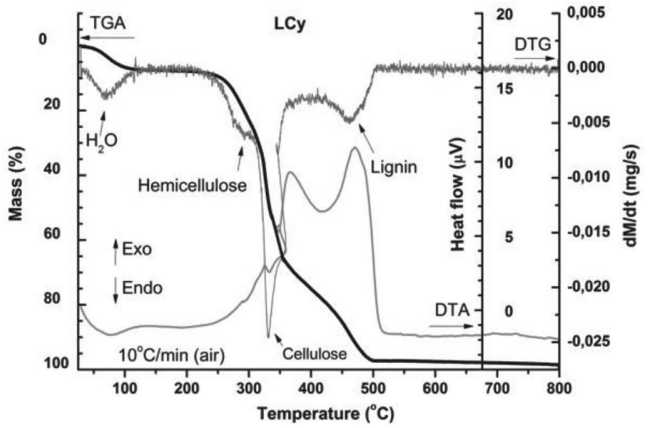

Fig. 8: Thermal decomposition of Luffa Cylindrica (LCy) at 10 K/min up to 800 °C in air. The black bold line represents the TG trace, the dark gray line is the time derivative of the mass DTG trace and the light gray line corresponds to the DTA trace.

Sintering the impregnated LCy samples at 1500 °C for 7 h in environmental atmosphere produced components with a porous microstructure (Fig. 9d), multidirectional ceramic fibrous array, and density of 3.21 g·cm^{-3} (80 % theoretical density). Fig. 9e shows a micrograph of the sintered fiber. The microstructure is composed of elongated grains with an average grain size of about 2 μm in length and 1 μm in width. Fig. 10f presents the micro-cellular structure formed by flocculated particles via CMC addition and by replica of cellular template morphology. When CMC dissolves in water, the macromolecules of A-COO$^-$ group can be adsorbed on two or more particles simultaneously. As a result, CMC long chains flocculate particles by bridging. Sintering green bodies composed of flocculated particles usually results in components with a porous microstructure.

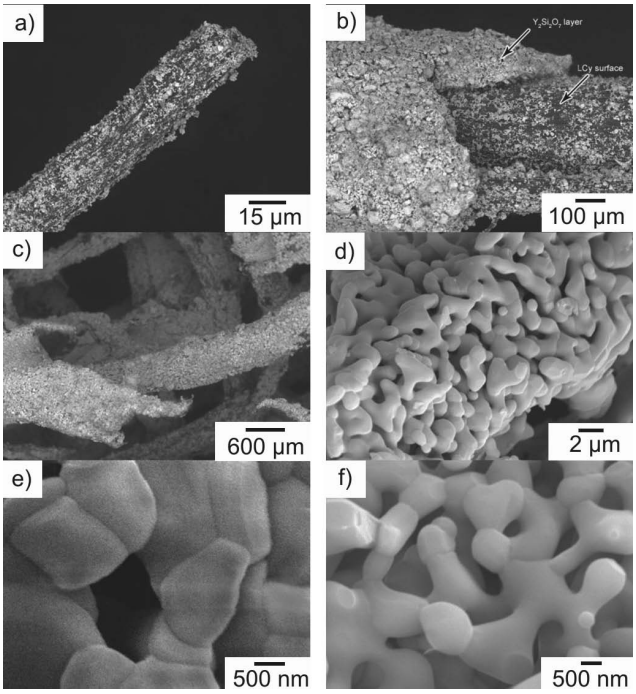

Fig. 9: Yttrium disilicate porous architecture by replica. LCy fiber impregnated with 25 vol% DsY suspension, (A) untreated fiber, (B) treated fiber showing the thickness of the impregnated ceramic layer, (C) impregnated LCy template; microstructure of LCy sponge sintered at 1500 °C/6 h in environmental atmosphere, (d) microporous fiber, (e) fiber surface and (e) fracture fiber surface.

Fig. 10 shows light emission spectra stimulated by DsY powder heating at 10 K/s up to 400 °C. The entire emission of the powders falls into the infrared range (λ = 750 – 4300 nm), with λ_{max} of 1000 nm at 400 °C behaving as a black body. As a solid is heated, it starts emitting continuous radiation at 200 °C and the intensity increases as a function of temperature. Entire radiation is invisible to human eyes (infrared and ultraviolet) and just a small fraction is in visible spectra. Unless doped with rare earths (RE:$Y_2Si_2O_7$), this compound does not emit visible light by itself.

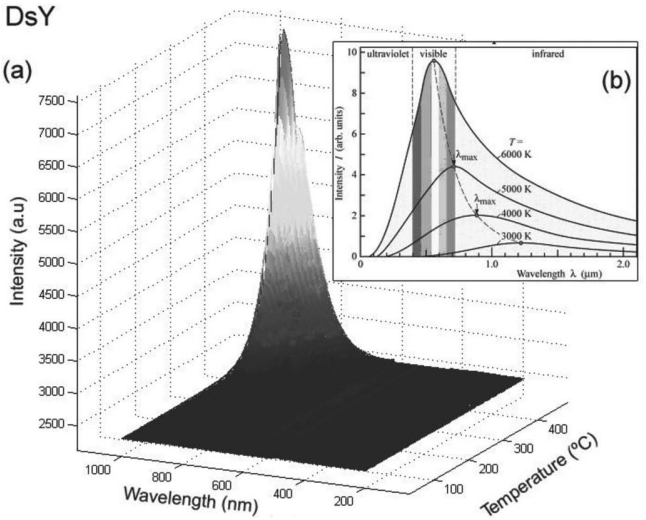

Fig. 10: Luminescence of solids as a function of temperature. (a) emission spectra of DsY powders heated at 10 °C/s up to 400 °C in environmental atmosphere; (b) emission spectra of solids based on Plank's law.

IV. Conclusions

Stable yttrium disilicate suspensions with 25 vol% solids load were prepared at pH 10 by using tetraethylammonium hydroxide and by adding 2 wt% polyelectrolyte. Suitable suspensions for the replica method could be prepared with 0.4 wt% CMC. The alkaline treatment of Luffa Cylindrica fibers with 2 mol% NaOH at 60 °C for 2 h was useful to remove any waxy and gummy substances from the surface of the fibers and to improve impregnation of the suspension into template. Sintering the impregnated vegetable samples at 1500 °C for 7 h in environmental atmosphere produced components with a porous microstructure, density of 3.21 g·cm^{-3} (80 % theoretical density) and morphology similar to biotemplating (multidirectional fibrous array). Thermoluminescence evaluation of the DsY powders showed that whole light emission occurred in the infrared range (λ = 750 – 4300 nm), showing a maximum wavelength of 1000 nm at 400 °C. Even though DsY presents no visible light emission, microstructural characteristics of replicas and intrinsic proprieties of DsY make it a potential material for gas burner technology.

Acknowledgements

The authors are deeply grateful to Dr Linda Caldas, Dr Maira Tiemi Yoshizumi, Dr Francisco Braga, Dr Thomaz Augusto Restivo, MSc. Douglas Will Leite, MSc. William Naville and Dr Wilson Acchar. In addition, their thanks also go to the State of São Paulo Research Foundation

(FAPESP), National Council for Scientific and Technological Development (CNPq), and High Degree People of Improvement Coordination (CAPES).

References

1 Ito, J., Johnson, H.: Synthesis and study of yttrialite, *Am. Mineral.,* **53**, 1940 – 1952, (1968).

2 Bataliev, N.G., Pyatenko, Y.A.: Artificial yttrialite (Y-Phase) – representative of a new structure type in rare-earth diorthosilicate series, *Sov. Phys. Crystallogr.,* **16**, 905 – 910, (1972).

3 Sun, Z.Q., Zhou, Y.C., Li, M.S.: Low-temperature synthesis and sintering of gamma-$Y_2Si_2O_7$, *J. Mater. Res.,* **21**, 1443 – 1450, (2006).

4 Maier, N., Rixecker, G., Nickel, K.G.: Formation and stability of Gd, Y, Yb and Lu disilicates and their solid solutions, *J. Solid State Chem.,* **179**, 1630 – 1635, (2006).

5 Parmentier, J., Bodart, P. R., Audoin, L., *et al.*: Phase transformations in gel-derived and mixed-powder-derived yttrium disilicate, $Y_2Si_2O_7$, by X-ray diffraction and Si-29 MAS NMR, *J. Solid State Chem.,* **149**, 16 – 20, (2000).

6 Leonyuk, N.I., Belokoneva, E.L., Bocelli, G., *et al.*: High-temperature crystallization and X-ray characterization of Y_2SiO_5, $Y_2Si_2O_7$ and $LaBSiO_5$, *J. Cryst. Growth,* **205**, 361 – 367, (1999).

7 Trusty, P.A., Chan, K.C., Ponton, C.B.: Synthesis of sinteractive single-phase microstructure yttrium disilicate precursor powder using hydrothermal processing, *J. Mater. Res.,* **13**, 3135 – 3143, (1998).

8 Moya, J.S., Díaz, M., Serna, C.J., *et al.*: Formation of nanocrystalline yttrium disilicate powder by an oxalate gel method, *J. Eur. Ceram. Soc.,* **18**, 1381 – 1384, (1998).

9 Christensen, A.N., Hazell, R.G., Hewat, A.W.: Synthesis, crystal growth and structure investigations of rare-earth disilicates and rare-earth oxyapatites, *Acta Chem. Scand.,* **51**, 37 – 43, (1997).

10 Kumar, S., Drummond, C.H.: Crystallization of various compositions in the Y_2O_3-SiO_2 system, *J. Mater. Res.,* **7**, 997 – 1003, (1992).

11 Bataliev, N.G., Bondar, I.A., Sidorenk, G.A., *et al.*: Synthetic silicate $Y_2Si_2O_7$, *Dokl. Akad. Nauk Sssr,* **173**, 339 ff., (1967).

12 Yamagata, C., Elias, D.R., Paiva, M.R.S., *et al.*: Facile preparation of apatite-type lanthanum silicate by a new water-based sol-gel process, *Mater. Res. Bull.,* **48**, 2227 – 2231, (2013).

13 Liddell, K., Thompson, D.P. : X-ray diffraction data for yttrium silicates, *Brit. Ceram. Trans. J.,* **85**, 17 – 22, (1986).

14 Diaz, M., Pecharroman, C., Del Monte, F., *et al.*: Synthesis, thermal evolution, and luminescence properties of yttrium disilicate host matrix, *Chem. Mater.,* **17**, 1774 – 1782, (2005).

15 Dilek, T., Koparan, E.T., Basoglu, M., *et al.*: The magnetic and structural properties of SiC-doped MgB(2) bulks prepared by the standard ceramic processing, *J. Supercond. Nov. Magn.,* **24**, 495 – 497, (2011).

16 Setz, L.F.G., Silva, A.C., Santos, S.C., *et al.*, A viscoelastic approach from α-Al_2O_3 suspensions with high solids content, *J. Eur. Ceram. Soc.,* **33**, 3211 – 3219, (2013).

17 Setz, L.F.G., Santacruz, I., Colomer, M.T., *et al.*: Tape casting of strontium and cobalt doped lanthanum chromite suspensions, *J. Eur. Ceram. Soc.,* **30**, 2897 – 2903, (2010).

18 Santos, S.C., Setz, L.F.G., Yamagata, C., *et al.*: Rheological study of yttrium oxide aqueous suspensions, *Mater. Sci. Forum VII,* **660 – 661**, 712 – 717, (2010).

19 Santos, S.C., Mello-Castanho, S.R.H.: Rheological behavior of yttria aqueous suspensions for impregnation method, presented at the CIMTEC- International Ceramic Congress, Montecatini Terme, Tuscany, 2010.

20 Kotani, Y., Behbahani, H.F., Takeno, T.: An excess enthalpy flame combustor for extended flow ranges, *Symposium (International) on Combustion,* **20**, 2025 – 2033, (1985).

21 Kotani, Y., Takeno, T.: An experimental study on stability and combustion characteristics of an excess enthalpy flame, *Symposium (International) on Combustion,* **19**, 1503 – 1509, (1982).

22 Wood, S., Harris, A.T.: Porous burners for lean-burn applications, *Prog. Energ. Combust.,* **34**, 667 – 684, (2008).

23 Luyten, J., Mullens, S., Cooymans, J., *et al.*: Different methods to synthesize ceramic foams, *J. Eur. Ceram. Soc.*, **29**, 829 – 832, (2009).

24 Studart, A.R., Gonzenbach, U.T., Tervoort, E., *et al.*: Processing routes to macroporous ceramics: A review, *J. Am. Ceram. Soc.,* **89**, 1771 – 1789, (2006).

25 Saggiowoyansky, J., Scott, C.E., Minnear, W.P.: Processing of porous ceramics, *Am. Ceram. Soc. Bull.,* **71**, 1674 – 1682, (1992).

26 Bowen, H.K.: Basic research needs on high-temperature ceramics for energy applications, *Mater. Sci. Eng.,* **44**, 1 – 56, (1980).

27 Nor, M.A.A.M., Hong, L.C., Ahmad, Z.A., *et al.*: Preparation and characterization of ceramic foam produced via polymeric foam replication method, *J. Mater. Process. Tech.,* **207**, 235 – 239, (2008).

28 Schwartzwalder, K., Somers, A.V.: Method of making porous ceramic, United States of America Patent, 1963.

29 Santos, S.C., Acchar, W., Yamagata, C., *et al.*: Yttria nettings by colloidal processing, *J. Eur. Ceram. Soc.,* **34**, 2509 – 2517, (2014).

30 Moreno, R., *Rheology of Ceramic Suspensions,* (in Spanish) , Madrid: Consejo superior de investigaciones científicas, (2005).

31 Liu, Z.T., Fan, T.X., Zhang, W., *et al.*: The synthesis of hierarchical porous iron oxide with wood templates, *Micropor.Mesopor. Mat.,* **85**, 82 – 88, (2005).

32 Sherman, A.J., Tuffias, R.H., Kaplan, R.B.: Refractory ceramic foams – a novel, new high-temperature structure, *Am. Ceram. Soc. Bull.,* **70**, 1025 – 1029, (1991).

33 Luyten, J., Thijs, I., Vandermeulen, W., *et al.*: Strong ceramic foams from polyurethane templates, *Adv.Appl. Ceram.,* **104**, 4 – 8, (2005).

34 Silva, S.A., Brunelli, D.D., Melo, F.C.L., *et al.*: Preparation of a reticulated ceramic using vegetal sponge as templating, *Ceram. Int.,* **35**, 1575 – 1579, (2009).

35 White, R.A., White, E.W., Weber, J.N.: Replamineform – new process for preparing porous ceramic, metal, and polymer prosthetic materials, *Science,* **176**, 922 ff., (1972).

36 Roy, D.M., Linnehan, S.K.: Hydroxyapatite formed from coral skeletal carbonate by hydrothermal exchange, *Nature,* **247**, 220 – 222, (1974).

37 Ben-Nissan, B.: Natural bioceramics: from coral to bone and beyond, *Curr. Opin.Solid St. M.,* **7**, 283 – 288, (2003).

38 Santos, S.C., Silva, A.C., Mello-Castanho, S.R.H., Morphology evolution of yttria porous ceramics during replica processing, *Mater. Sci. Forum,* (2011).

39 Rebouillat, S., Letellier, B., Steffenino, B.: Wettability of single fibres – beyond the contact angle approach, *Int. J. Adhes. Adhes.,* **19**, 303 – 314, (1999).

40 Kalnins, M.A.: Wettability of wood polymer composites – determination of contact-angle by modified wilhelmy plate method, *Abstr. Pap. Am. Chem. S.,* **194**, 64-Cell, (1987).

41 Lange, H.: Contact angle wettability and adhesion, *KolloidZ. Z. Polym.,* **204**, 134 ff., (1965).